EVALUATION OF LANDSAT-8 THERMAL BANDS TO MONITOR LAND SURFACE TEMPERATURE

Raquel NICLÒS CORTS[1], Juan M. SÁNCHEZ TOMÁS[2], José A. VALIENTE PARDO[3], Maria J. BARBERÀ BISBAL[1], Diego CASELLES MARTÍ[1], César COLL COMPANY[1], Vicente CASELLES MIRALLES[1]

[1] *Depto. Física de la Tierra y Termodinámica. Universidad de Valencia, C/Dr. Moliner 50, 46100 Burjassot, Valencia*

[2] *Depto. de Física Aplicada. Universidad de Castilla-La Mancha, Plz. Manuel Meca s/n, 13400 Almadén, Ciudad Real.*

[3] *Instituto Universitario Centro de Estudios Ambientales del Mediterráneo – CEAM-UMH, 14 Charles Darwin, 46980 Paterna, Valencia*

Raquel.Niclos@uv.es, Juanmanuel.Sanchez@uclm.es, valiente_jospar@gva.es, m.jesus.barbera@uv.es, Diego.Caselles@uv.es, Cesar.Coll@uv.es, Vicente.Caselles@uv.es

RESUMEN

El nuevo Thermal Infrared Sensor (TIRS) a bordo del Landsat-8 (L8) dispone de dos bandas térmicas, 10 (11.60-11.19 μm) y 11 (11.50-12.51 μm), con una resolución espacial de 100m, con el fin de proporcionar temperaturas de la superficie terrestre (LST) de una manera más precisa que su predecesor Landsat-7 ETM+. El L8 fue lanzado en febrero de 2013, comenzando su adquisición operativa a mediados de abril. Los primeros estudios realizados por el equipo de calibración de L8 mostraron errores sistemáticos significativos para el TIRS, y en febrero de 2014 el archivo de imágenes L8 TIRS fue reprocesado para corregir dichos errores. En este estudio, con el fin de comprobar la calibración del L8 TIRS, realizamos medidas de campo en una zona llana y térmicamente homogénea dedicada al cultivo del arroz. A partir de estas medidas de LST simulamos las radiancias y temperaturas de brillo a nivel del satélite y las comparamos con los datos TIRS. Tal y como apuntaba el equipo de L8, nuestros resultados muestran una sobreestimación para la banda 11. Sin embargo, el recalibrado aplicado por dicho equipo para ambas bandas ha resultado no ser satisfactorio en nuestra zona experimental, ya que proponen sustraer errores sistemáticos mayores a los requeridos.

Palabras clave: Landsat-8, Infrarrojo Térmico, Temperatura de la Superficie Terrestre, Calibración.

ABSTRACT

The new Landsat-8 (L8) Thermal Infrared Sensor (TIRS) has two thermal bands, 10 (11.60-11.19 μm) and 11 (11.50-12.51 μm) at 100-m spatial resolution, aimed to provide more accurate Land Surface Temperatures (LST) than Landsat-7 ETM+. L8 was launched on February 2013, and operational acquisitions started in middle April 2013. The first studies by the L8 Calibration Team showed significant TIRS temperature offsets, and in February 2014 the L8 TIRS archive was reprocessed to remove these offsets. In this study, ground LST measurements were performed in a flat and thermally homogeneous area of rice-crop fields for checking the calibration of the L8 TIRS bands. At-sensor radiances and brightness temperatures were simulated from ground-measured LSTs and compared with TIRS values. A significant overestimation was observed for band 11, in agreement with the L8 Calibration

Team results. However, their recalibration was shown unsatisfactory in our test site for both bands, since they proposed subtracting higher offsets than required.

Keywords: Landsat-8, Thermal Infrared, Land Surface Temperature, Calibration.

1. INTRODUCTION

For the past 40 years Landsat satellites have been providing multispectral global observations of the Earth surface at high spatial resolution. Landsat 7 (launched in 1999) is still operational and continues to provide useful measurements with the Enhanced Thematic Mapper+ (ETM+) instrument. ETM+ includes a band in the thermal infrared (TIR) region (band 6, 10.31-12.36 μm) with spatial resolution of 60 m. Landsat system has never provided an operational land surface temperature (LST) product because of the limitation of the single thermal band to correct for atmospheric and emissivity effects since atmospheric profiles of temperature and water vapor measured concurrently to the satellite overpass are necessary as inputs of a radiative transfer code, together with surface emissivity data. Also, a failure in the scan line corrector (SLC) occurred in 2003. Even though Landsat 7 ETM+ continues to acquire image data in the "SLC-off" mode with the same high radiometric and geometric quality as data collected prior to the SLC failure, gaps and overlaps between successive scans reduce the coverage of the scene from none at the center of the scan to 14 pixels at the edge of the scan (Markham et al. 2004).

With the intent to overcome some of the previous issues the Landsat Data Continuity Mission (LDCM), renamed Landsat-8 (L8), was launched on February 2013, and operational acquisitions started middle April 2013. The L8 Thermal Infrared Sensor (TIRS) has two thermal bands, 10 (11.60-11.19 μm) and 11 (11.50-12.51 μm), aimed to provide more accurate Land Surface Temperatures (LST) than the Landsat-7 ETM+, at 100-m spatial resolution. Thermal data are provided as calibrated at-sensor (top-of-atmosphere) radiances that can be converted to equivalent brightness temperatures.

Since the first Earth observation satellite with thermal infrared bands, the Heat Capacity Mapping Mission (HCMM), calibration errors have been observed after satellite launch (Caselles et al. 1983). The on-board calibration of Landsat series thermal bands has been continuously monitored using lakes as vicarious calibration targets. For instance, according to vicarious calibration over lakes in 1999-2007, the ETM+ thermal band appears to be stable and calibrated within ±0.6 K after the correction of an offset error in late 2000 (Barsi, 2007). In an analogous task the first studies showed TIRS temperature offsets for L8, and in November 2013 the L8 calibration team proposed subtracting 0.29 ± 0.12 $Wm^{-2}sr^{-1}\mu m^{-1}$ (~2.1 ± 0.8 K) and 0.5 ± 0.2 $Wm^{-2}sr^{-1}\mu m^{-1}$ (~4.4 ± 1.8 K) from radiances measured by band 10 and 11, respectively, with a root mean square variability for the recalibration of ±0.12 $Wm^{-2}sr^{-1}\mu m^{-1}$ (±0.8 K) and ±0.2 $Wm^{-2}sr^{-1}\mu m^{-1}$ (±1.8 K) for bands 10 and 11, respectively (http://landsat.usgs.gov/calibration_notices.php). The offsets represent an average error introduced by stray light coming from outside the TIRS field of view for temperatures between 10-30 ºC. Due to the larger calibration uncertainty associated with band 11, it was recommended that users refrain from relying on band 11 data in quantitative analysis of the TIRS data, such as the use of split window techniques for atmospheric correction and retrieval of surface temperatures. On February 3, 2014, the entire L8 archive was reprocessed to remove these calibration offsets (TIRS digital numbers being modified).

The aim of this study is to contribute to the TIRS calibration efforts using ground transect measurements of Land Surface Temperature (LST), concurrent to L8 overpasses, performed in a ~100 km^2, flat and thermally homogeneous area of rice-crop fields (39.267ºN, -0.308ºE in

WGS-84, at sea level) close to Valencia-Spain. The Valencia test site has been used in previous studies, with its thermal homogeneity being assessed at different spatial scales for full vegetation cover (Coll et al. 2005, 2007, 2010; Niclòs et al. 2011). For the present work, beyond the fully vegetated surface conditions, flooded soil (water surface) and bare soil covers were considered instead (see Figure 1), to enlarge the LSTs range from around 10 ºC to 40 ºC, and account for a variety of environmental conditions.

A set of six L8 scenes was used in this work. Atmospheric profiles from the National Center for Environmental Prediction (NCEP) were used as inputs into MODTRAN 5 model (Berk et al. 2006) to estimate the atmospheric parameters required. In situ emissivity measurements were also conducted for the different surface conditions.

Fig. 1: Views of the Valencia Test Site on two different dates: 01/27/2014, flooded soil (left) and 05/03/2014, bare soil (right).

2. DATA AND METHODOLOGY

2.1 L8 TIRS data

Six daytime Landsat 8 scenes were acquired over the Valencia Test Site between January and June 2014 (see Table 1 and Fig. 2). The location of the Valencia Test Site falls within two different L8 paths (198 and 199) and a single row (33). This allows doubling the L8 captures increasing the revisit time to 7-8 days, although the cloudy events at the test site limited the available data for the study period.

Scenes were downloaded from the United States Geological Survey EROS Data Center (earthexplorer.usgs.gov). Landsat thermal band data are given as 16-bit digital numbers (DN) that are calibrated to at-sensor radiances ($L_{sen,i}$) as:

$$L_{sen,i} = M_{Li}\, DN_i + A_{Li} \tag{1}$$

where M_{Li} are band-specific multiplicative rescaling factors, and A_{Li} are band-specific additive rescaling factors (see Table 2). The brightness temperature, T_{bi}, is obtained from the at-sensor radiance as:

$$T_{bi} = \frac{k_{2i}}{\ln\left(\frac{k_{1i}}{L_{sen,i}} + 1\right)} \tag{2}$$

where k_{1i} and k_{2i} are band-specific thermal conversion constants (Table 2).

The processing level of the scenes was L1T, which provides systematic radiometric and geographic accuracy using ground control points and digital elevation model as well. Data were collected at 100 m spatial resolution but resampled to match the OLI spectral bands using cubic convolution to 30 m. The scenes were geo-referenced with sufficient accuracy to identify correctly the pixels corresponding to the test site. We checked that the area around the test site was cloud-free by visual inspection of the reflective and thermal bands.

Table 1. Date and time of the L8 scenes used in this study.

Case	Date	UTC Time (h:m)	path/row	Surface condition
1	January 27	10:45	199/33	Flooded
2	February 12	10:44	199/33	Wet bare soil
3	March 16	10:44	199/33	Dry bare soil (non-tilled)
4	April 10	10:37	198/33	Dry bare soil (tilled)
5	May 3	10:43	199/33	Dry bare soil (tilled)
6	June 4	10:43	199/33	Flooded

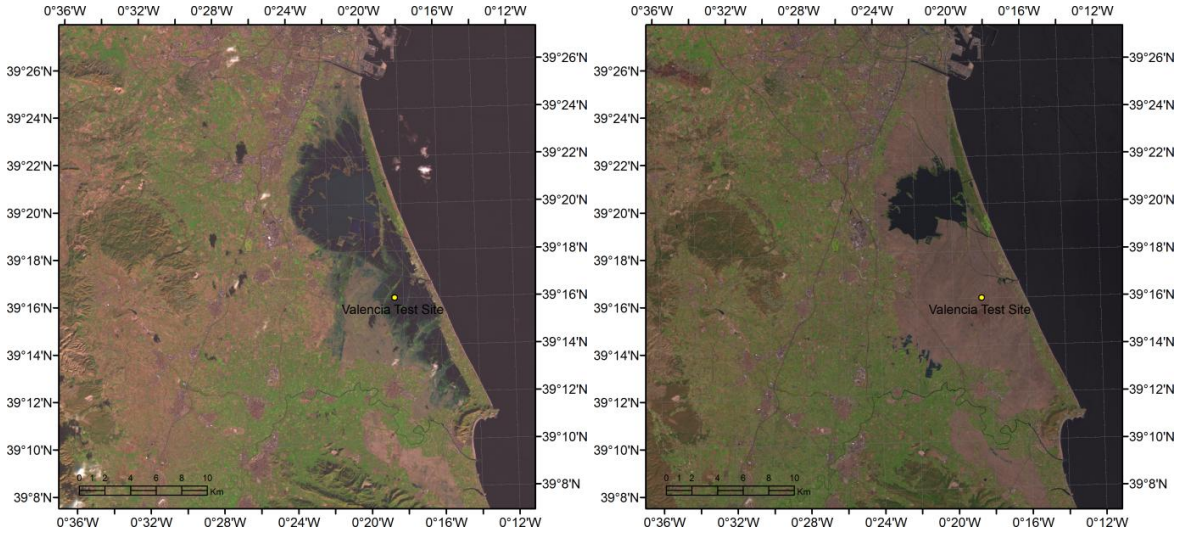

Fig. 2. False color composite (6,5,4) of the L8 images on 01/27/2014 (left) and 05/03/2014 (right). The point shows the exact location of the test site.

Table 2. Band-specific rescaling factors, and thermal conversion constants.

TIRS band i	M_{Li}	A_{Li}	k_{1i}	k_{2i}
10	0.000334	0.1	774.89	1321.08
11	0.000334	0.1	480.89	1201.14

2.2 Ground LST measurements

Four TIR radiometers were used to perform the transects: two CIMEL CE 312-1 with four bands (8–13, 11.5–12.5, 10.5–11.5, and 8.2–9.2 μm) and two CIMEL CE 312-2 with six bands (8–13, 8.1–8.5, 8.5–8.9, 8.9–9.3, 10.3–11.0, and 11.0–11.7 μm) (www.cimel.fr). Before and after each field measurement, the instruments were calibrated against a LANDCAL P80P blackbody source (www.landinst.com). The CE 312 radiometers showed uncertainties within ±0.2 K for all bands at 20–30 °C. The radiometers were carried back and forth along transects of 100 m in length, and temperatures measured within 3 min centered at the satellite overpass

time were averaged as a compromise between sufficient sampling and not introducing too much temporal variability.

Downwelling sky randiance was also measured to account for the atmospheric correction of the ground measurements. Emissivity measurements were also performed in field conditions using different techniques depending on the land cover on the L8 acquisition date: the Temperature-Emissivity Separation (TES) method (Sánchez et al., 2011), the Box Method (Rubio et al., 2003), and a portable infrared Designs & Prototypes 102 spectroradiometer (2–16 μm) (www.dpinstruments.com). The TES method was used especially in the case of bare soil due to the relatively high emissivity spectral variation between 8 to 14μm and taking the angular variation of the bare soil emissivity into account (García-Santos et al., 2012a). The method was used with the CE 312-2 radiometers at nadir. The D&P spectroradiometer was used to test the performance of the TES derived emissivities. Figure 3 shows an example of the emissivities measured with the D&P spectroradiometer (mean value of 400 scans) and the TES method processed using CE 312-2 measurements for the bare soil of the test site (silty clay loam, see properties for sample D in García-Santos et al. (2012a)) on April 10, 2014. Water surface emissivities considered for flooded surface conditions were obtained from Niclòs et al. (2005; 2009; 2014).

The CE 312-1 (CE 312-2) measurements at the 10.5–11.5 μm (10.3-11.0 μm) band were finally used to obtain the LST since atmospheric effects and emissivity uncertainties are the lowest for this spectral region. The standard deviation of the ground LSTs in each transect was calculated as a measure of the spatial and temporal LST variability and the quadratic sum of this deviation and the standard deviation of the data measured by the four radiometers was used to show the variability in the test site (from ±0.3K to ±1.7K). Together with the mean ground LST, LST_g, we estimated the total LST uncertainty, which includes the calibration error of the radiometers, the emissivity correction error, and the LST variability (see section 3).

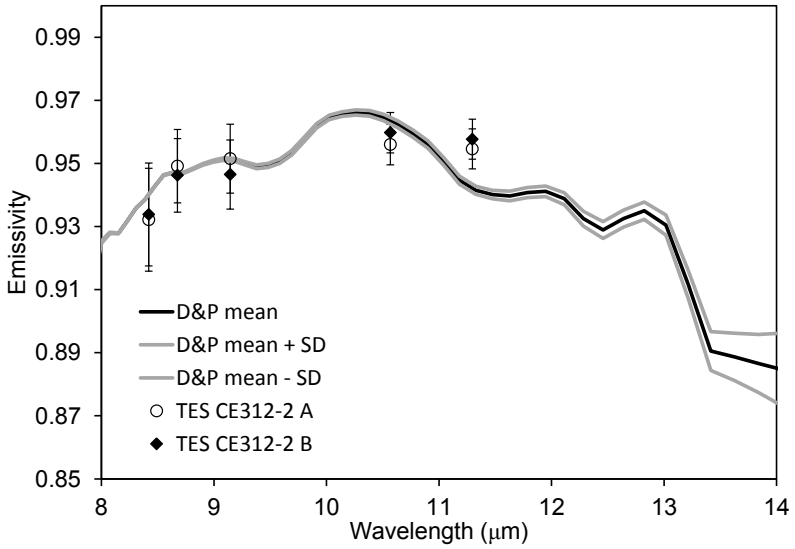

Fig. 3: Comparison between the emissivity data measured for the site bare soil with the D&P spectroradiometer (mean and standard deviation, SD, of 400 scans), and using two CE312-2 radiometers and applying the TES method to their data.

2.3 Methodology: Radiative transfer calculations

The MODTRAN-5 radiative transfer model (Berk et al., 2006), together with re-analysis atmospheric profiles from the National Center for Environmental Prediction (NCEP), interpolated to the site location, date and time, were used to calculate the atmospheric transmittance and emitted radiance in the spectral range of the L8 TIR bands.

Atmospheric transmittance (τ_λ) and radiance emitted towards the sensor ($L_\lambda^\uparrow$) were obtained at nadir. We also calculated the downwelling atmospheric radiance, $L_\lambda^\downarrow(\theta)$, at twelve zenith angles from θ=0º to 89º, which were used to obtain the hemisphere-integrated downwelling radiance:

$$L_\lambda^\downarrow = \frac{1}{\pi}\int_0^{2\pi}\int_0^{\pi/2} L_\lambda^\downarrow(\theta)\cos\theta \,\mathrm{sen}\theta \, d\theta \, d\varphi \quad (3)$$

where no dependence on the azimuth angle is assumed for clear skies and horizontally homogeneous atmospheres.

The radiance measured by the sensor, L_i, can be simulated using the atmospheric transmittance and emitted radiances (forward simulation). For a surface at temperature LST and with emissivity ε_λ we can write:

$$L_i = \int_0^\infty f_i(\lambda)\,\{[\varepsilon_\lambda B_\lambda(LST) + (1-\varepsilon_\lambda)L_\lambda^\downarrow]\tau_\lambda + L_\lambda^\uparrow\}\,d\lambda \quad (4)$$

where B_λ is the Planck function for blackbody spectral radiance and $f_i(\lambda)$ is the normalized spectral response function of band i ($\int_0^\infty f_i(\lambda)d\lambda = 1$). Lambertian reflection is assumed in (4).

An approximate expression can be used if the spectral magnitudes in (4) are converted to band-averaged magnitudes (B_i, ε_i, τ_i, $L_i^\uparrow$, and $L_i^\downarrow$):

$$L_i = [\varepsilon_i B_i(LST) + (1-\varepsilon_i)L_i^\downarrow]\tau_i + L_i^\uparrow \quad (5)$$

The brightness temperature, T_{bi}, corresponding to the simulated at-sensor radiance L_i was calculated using (2). The T_{bi} is usually lower than the LST in (5) due to atmospheric and emissivity effects.

Equation (5), with τ_i=1 and $L_i^\uparrow$=0, was used to correct the ground measurements from emissivity and downwelling radiance effects. The surface emissivities required to correct ground data with (5) were measured in field conditions as explained in section 2.2. The hemisphere-integrated downwelling radiance defined by (3) was calculated as the radiance measured by the CE 312 radiometers at zenith multiplied by a factor (of around 1.5) dependent on the spectral band and the atmospheric water vapor content (García-Santos et al. 2012b), which was estimated from the NCEP profiles.

Equation (5) was also used to derive the LST from the satellite-measured at-sensor radiance L_i (inverse simulation).

3. RESULTS AND DISCUSSION

Ground measurements were compared with L8 TIRS data for a vicarious calibration of bands 10 and 11. This comparison was performed in terms of: a) L8 TIRS at-sensor brightness

temperatures, T_{bi}, and radiances, L_i (forward simulation), and b) at-surface temperatures, LSTs (inverse simulation). In the first case, L8 TIRS L_i values were simulated using (5) with LST being the ground-measured temperature. The atmospheric parameters required in (5) were simulated for the TIRS bands using NCEP atmospheric profiles and the MODTRAN 5 model as explained in section 2.3. Emissivity values for the L8 TIRS bands were estimated for each surface condition from the CE 312-1 (CE 312-2) measurements, described in section 2.2, at the 10.5–11.5 μm (10.3-11.0 μm) and 11.5–12.5 μm (11.0-11.7 μm) bands, respectively (see latter in Table 5).

Table 3 shows the ground-measured LSTs, LST_g, and the L_i and T_{bi} simulated for L8 TIRS band 10 and 11 from them, together with the L8 TIRS acquired values. With the purpose of calibrating the original data acquired by the L8 TIRS, the TIRS data after February 3, 2013, were obtained adding the recalibration radiance offsets given by the L8 Calibration Team (0.29 ± 0.12 $Wm^{-2}sr^{-1}\mu m^{-1}$ and 0.5 ± 0.2 $Wm^{-2}sr^{-1}\mu m^{-1}$ for band 10 and 11 respectively), since DNs in TIRS images were modified with the reprocessing applied to the L8 image archive from this date. L8 TIRS data shown in Table 3 were obtained from the mean and standard deviation of the DNs in a 17 x 17 pixel array around the geographic coordinates of the test site. Since TIRS data are resampled from 100m to 30m, a 17 x 17 pixel array was used to cover the extension of 5 x 5 original pixels. Very similar results were obtained for one pixel due to the thermal homogeneity of the experimental site, as the low spatial variation in 17 x 17 pixel shown in terms of T_{bi} proves (< 0.4 K in all cases). Figure 4 shows L_i simulated from LST_g against L8 TIRS L_i for both thermal bands, together with linear regression equations that can be used as recalibration equations to adjust L8 TIRS L_i. Table 4 shows the statistical results (mean (bias), standard deviation (SD) and quadratic sum of bias and SD (RMSE)) of the differences between L_i and T_{bi} values measured by the L8 TIRS and simulated from LST_g data, both for 17 x 17 pixels and 1 pixel.

Table 3. Ground-measured LSTs, LST_g, together with the L8 TIRS values.

Case	Ground data	L8 TIRS data			
	LST_g (°C)	L_{10} ($W\ m^{-2}\ sr^{-1}\ \mu m^{-1}$)	T_{b10} (°C)	L_{11} ($W\ m^{-2}\ sr^{-1}\ \mu m^{-1}$)	T_{b11} (°C)
1	12.7±0.3	7.68	12.5	7.36	13.2
2	15.3±0.6	7.75	13.1	7.43	13.8
3	27.6±1.3	9.17	23.8	8.62	24.2
4	36.8±1.7	9.99	29.6	9.25	29.4
5	40.1±1.1	10.88	35.5	9.97	35.1
6	30.6±0.9	9.67	27.4	8.96	27.0

Table 4. Statistical results of the differences between L_i and T_{bi} values measured by the L8 TIRS and simulated from LST_g (for 17 x 17 pixel array and 1 pixel).

	17 x 17 pixel				1 pixel			
	L_{10} ($W\ m^{-2}\ sr^{-1}\ \mu m^{-1}$)	T_{b10} (°C)	L_{11} ($W\ m^{-2}\ sr^{-1}\ \mu m^{-1}$)	T_{b11} (°C)	L_{10} ($W\ m^{-2}\ sr^{-1}\ \mu m^{-1}$)	T_{b10} (°C)	L_{11} ($W\ m^{-2}\ sr^{-1}\ \mu m^{-1}$)	T_{b11} (°C)
bias	0.06	0.5	0.27	2.3	0.06	0.4	0.27	2.3
SD	0.09	0.6	0.08	0.7	0.11	0.8	0.09	0.7
RMSE	0.11	0.8	0.28	2.4	0.13	0.9	0.29	2.4

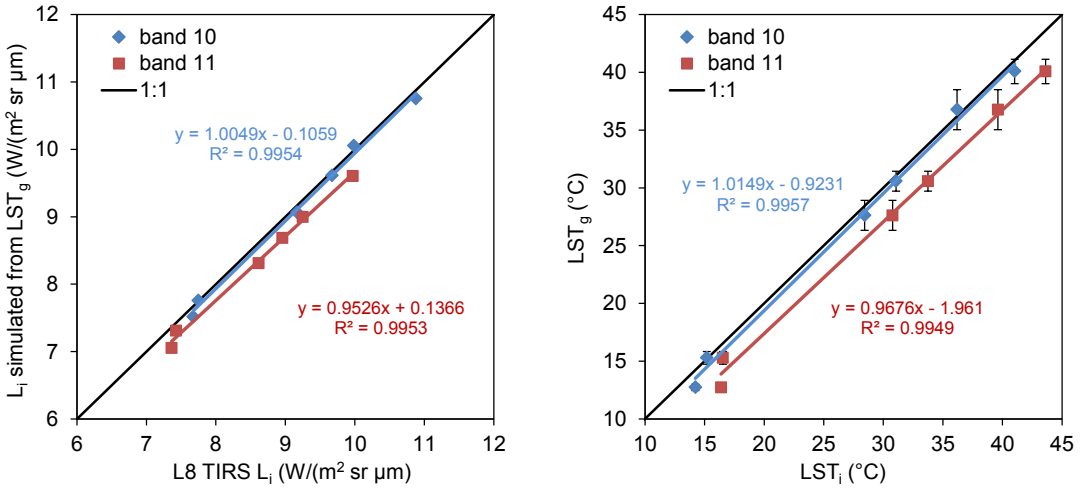

Fig. 4: Radiances simulated from LST_g against L8 TIRS radiances for band 10 and 11, (left) and ground-measured LST_g against LST_i obtained from the L8 TIRS radiances (right), together with linear regression equations.

As shown in Figure 4 and Table 4, L8 TIRS L_{10} and T_{b10} are just slightly higher than those simulated from LST_g in the Valencia Test Site, with differences of 0.06 ± 0.09 W m^{-2} sr^{-1} μm^{-1} in L_{10} and 0.5 ± 0.6 K in T_{b10}, instead of 0.29 ± 0.12 $Wm^{-2}sr^{-1}\mu m^{-1}$ and ~2.1 ± 0.8 K estimated with ground data measured in water bodies by the L8 Calibration Team. However, a significant L8 TIRS overestimation is observed for band 11, with differences of 0.27 ± 0.08 W m^{-2} sr^{-1} μm^{-1} in L_{11} and 2.3 ± 0.7 K in T_{b11}. The L8 Calibration Team also pointed out the existence of a significant offset in band 11 data, which was even larger than the values obtained in our site (0.5 ± 0.2 $Wm^{-2}sr^{-1}\mu m^{-1}$ and ~4.4 ± 1.8 K).

The comparison between L8 TIRS data and ground measurements was also performed in terms of at surface temperature LST (inverse simulation). In this case, TIRS radiances were corrected for the emissivity and atmospheric effects, with the parameters simulated with MODTRAN 5 and NCEP profiles, to obtain a LST value from each band, LST_i, by solving (5) for LST. The obtained LSTs were compared with the ground-measured LSTs, LST_g. Table 5 shows the LSTs obtained from the TIRS data (see Table 3), together with the emissivity values used in each case, depending on the land cover, for which uncertainties of ±0.007 were obtained. L_i values of 17x 17 pixels are used in this case, with very similar values for one pixel. Figure 4 also shows LST_g against LST_i obtained from the L8 TIRS radiances, together with linear regression equations. In general, LST results for both bands overestimate the ground data, which range from ~10°C to ~40°C. A mean difference of 0.5 ± 0.8 K (with RMSE of ± 0.9 K) was obtained for band 10. Larger overestimations were obtained for band 11, with a mean difference of 2.9 ± 0.9 K (with RMSE of ± 3.1 K). In this case, statistical results were exactly equal for 17 x 17 pixels and for one pixel.

4. CONCLUSIONS

At-sensor radiances and brightness temperatures were simulated for the L8 TIRS band 10 and 11 from ground LST measurements taken in the Valencia Test Site with different surface conditions given by the rice-crop phenology. They were compared with the L8 TIRS data acquired over the test site on six dates from January to June 2014. Significant differences

between L8 TIRS data and simulated values from ground LST were obtained, which showed L8 TIRS overestimations for both thermal bands, specially significant for band 11, in agreement with the L8 Calibration Team results. For band 10, a slight radiance overestimation of 0.06 ± 0.09 W m^{-2} sr^{-1} μm^{-1}, and 0.5 ± 0.6 K in terms of brightness temperatures, was obtained in the Valencia Test Site, instead of the radiance and temperature offsets of 0.29 ± 0.12 $Wm^{-2}sr^{-1}\mu m^{-1}$ and ~2.1 ± 0.8 K, respectively, estimated in water bodies by the L8 Calibration Team. For band 11, the radiance overestimation was 0.27 ± 0.08 W m^{-2} sr^{-1} μm^{-1}, and 2.3 ± 0.7 K in brightness temperature, which is lower than the radiance offset given by the L8 Calibration Team (0.5 ± 0.2 $Wm^{-2}sr^{-1}\mu m^{-1}$; ~4.4 ± 1.8 K in temperature). The same conclusions can be drawn by comparing the data in terms of LSTs. LSTs were obtained from L8 TIRS band 10 and 11 radiances after correcting the atmospheric and emissivity effects. The results were compared with ground-measured LSTs from ~10°C to ~40°C. Mean differences between LSTs simulated from L8 TIRS radiances and ground LSTs of 0.5 ± 0.8 K (with RMSE of ± 1.0 K) and 2.9 ± 0.9 K (with RMSE of ± 3.1 K) were obtained for bands 10 and 11, respectively. Therefore, we confirm that L8 TIRS band 11 data requires a recalibration. However, the recalibration proposed by the L8 Calibration Team for band 10 and 11 was shown unsatisfactory in our test site, since they proposed subtracting higher offsets than required. In fact, after the reprocessing in February 2013, L8 TIRS data underestimate ground-measured temperatures in the Valencia Test Site (~2.0 ± 0.8 K and ~2.7 ± 0.9 K for bands 10 and 11, respectively, in terms of LST).

Table 5. LSTs obtained from the TIRS radiances in band 10 and 11 after emissivity and atmospheric corrections, together with the emissivities used in each case.

Case	ε_{10}	ε_{11}	LST_{10} (°C)	LST_{11} (°C)
1	0.991	0.985	14.2	16.4
2	0.977	0.978	15.2	16.5
3	0.959	0.959	28.4	30.8
4	0.958	0.956	36.2	39.6
5	0.969	0.963	41.0	43.6
6	0.991	0.985	31.1	33.7

5. ACKNOWLEDGMENTS

This study was supported by the Spanish Ministerio de Economía y Competitividad (projects CGL2010-16364, CGL2010-17577/CLI, CGL2011-13579-E, CGL2011-30433 and GRACCIE Consolider–Ingenio 2010; and Dr. Niclòs' "Ramón y Cajal" Research Contract) and Generalitat Valenciana (PROMETEO/2009/006 and PROMETEO/2009/086 projects). The Instituto Universitario CEAM-UMH is partly supported by the Generalitat Valenciana. The authors thank the assistance of the students involved in the experimental campaign.

6. REFERENCES

Barsi, J. A., B. L. Markham, D. L. Helder, and G. Chander. (2007). "Radiometric calibration status of Landsat-7 and Landsat-5," *Sensor, Systems and Next-Generation Satellites*. Proceedings of SPIE, vol. 6744, pp. 67441F.

Berk, A., G.P. Anderson, P.K. Acharya, L.S. Bernstein, L. Muratov, J. Lee, M. Fox, S.M. Adler-Golden, J.H. Chetwynd, M.L. Hoke, R.B Lockwood, J.A. Gardner, T.W. Cooley, C.C.

Borel, P.E. Lewis and E.P. Shettle. (2006). "MODTRAN5: 2006 Update," Proc. SPIE, Vol. 6233, 62331F.

Caselles, V., Gandia, V., and Meliá, J. (1983). "Significance of apparent temperature measurements carried out by the HCMM satellite over areas of vegetation". *Agricultural Meteorology*, 30, 77-82.

Coll, C., V. Caselles, J. M. Galve, E. Valor, R. Niclòs, J. M. Sánchez, and R. Rivas. (2005). "Ground measurements for the validation of land surface temperatures derived from AATSR and MODIS data". *Remote Sensing of Environment*, 97, 288-300.

Coll, C., V. Caselles, E. Valor, R. Niclòs, J.M. Sánchez, J.M. Galve, and M. Mira. (2007). "Temperature and emissivity separation from ASTER data for low spectral contrast surfaces". *Remote Sensing of Environment*, 110, 162-175.

Coll, C., J.M. Galve, J.M. Sánchez, and V. Caselles. (2010). "Validation of Landsat 7/ETM+ thermal band calibration and atmospheric correction with ground-based measurements". *IEEE Transactions on Geoscience and Remote Sensing.,* vol. 48, no. 1, pp. 547-555, Jan 2010.

García-Santos, V., E. Valor, V. Caselles, M.A. Burgos, and C. Coll. (2012a). "On the angular variation of thermal infrared emissivity of inorganic soils". *Journal of Geophysical Research*, 117, D19116, doi:10.1029/2012JD017931.

García-Santos, V., J.M. Galve, E. Valor, V. Caselles, and C. Coll (2012b). "Estimation of atmospheric water vapour content from direct measurements of radiance in the thermal infrared region." *Remote Sensing Letters*, 3(1).

Markham, B.L., J. C. Storey, D. L. Williams, and J. R. Irons. (2004). "Landsat sensor performance: History and current status". *IEEE Transactions on Geoscience and Remote Sensing*, 42, 2691-2694.

Niclòs, R., E. Valor, V. Caselles, C. Coll, and J. M. Sánchez (2005). "In situ angular measurements of thermal infrared sea surface emissivity—Validation of models". *Remote Sensing of Environment,* 94, 83–93.

Niclòs, R., V. Caselles, E. Valor, C. Coll, and J. M. Sanchez. (2009). "A simple equation for determining the sea surface emissivity in the 3–15 μm region". *International Journal of Remote Sensing,* 30, 1603–1619.

Niclòs, R., J.M. Galve, J.A. Valiente, M.J. Estrela, and C. Coll (2011). "Accuracy assessment of land surface temperature retrievals from MSG2-SEVIRI data". *Remote Sensing of Environment,* 115, 2126-2140.

Niclòs R., Doña, C., Valor, E. and Bisquert, M. (2014). "Thermal-Infrared Spectral and Angular Characterization of Crude Oil and Seawater Emissivities for Oil Slick Identification". *IEEE Transactions on Geoscience and Remote Sensing*, 52(9).

Rubio, E., Caselles, V., Coll, C., Valor, E., and Sospedra, F. (2003). "Thermal-infrared emissivities of natural surfaces: Improvements on the experimental set-up and new measurements". *International Journal of Remote Sensing*, 24(24), 5379–5390.

Sánchez, J.M., A.N. French, M. Mira, D.J. Hunsaker, K.R. Thorp, E. Valor, and V. Caselles. (2011). "Thermal infrared emissivity dependence on soil moisture in field conditions". *IEEE Transactions on Geoscience and Remote Sensing.,* 49, pp. 4652-4659.